

**Phase synchronization of bursting neurons in clustered small-world networks**C. A. S. Batista,<sup>1</sup> E. L. Lameu,<sup>1</sup> A. M. Batista,<sup>2</sup> S. R. Lopes,<sup>3</sup> T. Pereira,<sup>4</sup> G. Zamora-López,<sup>5,6</sup> J. Kurths,<sup>6,7,8</sup> and R. L. Viana<sup>3,\*</sup><sup>1</sup>Graduate Program in Physics, State University of Ponta Grossa, Ponta Grossa, Paraná, Brazil<sup>2</sup>Department of Mathematics and Statistics, State University of Ponta Grossa, Ponta Grossa, Paraná, Brazil<sup>3</sup>Department of Physics, Federal University of Paraná, Curitiba, Paraná, Brazil<sup>4</sup>Department of Mathematics, Imperial College, London, London SW7 2AZ, United Kingdom<sup>5</sup>Bernstein Center for Computational Neuroscience, Berlin, Germany<sup>6</sup>Department of Physics, Humboldt University, Berlin, Germany<sup>7</sup>Institute for Complex Systems and Mathematical Biology, Aberdeen, Scotland<sup>8</sup>Potsdam Institute for Climate Impact Research, Potsdam, Germany

(Received 30 March 2012; published 13 July 2012)

We investigate the collective dynamics of bursting neurons on clustered networks. The clustered network model is composed of subnetworks, each of them presenting the so-called small-world property. This model can also be regarded as a network of networks. In each subnetwork a neuron is connected to other ones with regular as well as random connections, the latter with a given intracluster probability. Moreover, in a given subnetwork each neuron has an intercluster probability to be connected to the other subnetworks. The local neuron dynamics has two time scales (fast and slow) and is modeled by a two-dimensional map. In such small-world network the neuron parameters are chosen to be slightly different such that, if the coupling strength is large enough, there may be synchronization of the bursting (slow) activity. We give bounds for the critical coupling strength to obtain global burst synchronization in terms of the network structure, that is, the probabilities of intracluster and intercluster connections. We find that, as the heterogeneity in the network is reduced, the network global synchronizability is improved. We show that the transitions to global synchrony may be abrupt or smooth depending on the intercluster probability.

DOI: [10.1103/PhysRevE.86.016211](https://doi.org/10.1103/PhysRevE.86.016211)

PACS number(s): 05.45.Xt, 87.19.II, 87.19.lm

**I. INTRODUCTION**

The human brain is a complex network consisting of approximately  $10^{11}$  neurons, linked together by  $10^{14}$  to  $10^{15}$  connections, amounting to nearly  $10^4$  synapses per neuron [1]. The connection architecture of the brain is very complicated, and neurons are neither completely nor randomly connected. However, neuroanatomic studies reveal that neurons with similar connectional and functional features are grouped into clusters with  $10^5$  to  $10^6$  cells with spatial localization. Such clusters form structures called cortical areas or subcortical nuclei [2,3].

Accurate maps of neural anatomic connectivity are difficult to achieve. Current anatomical data for a few species are available, for example, the large-scale connectivity between cortical areas in the macaque monkeys and cats, and the complete neural connectivity of the worm *Caenorhabditis elegans* [4–7]. Another source of data for connectivity studies relies in the statistical or dynamical relationship between the patterns of activation of different brain regions as measured by electroencephalographic (EEG) or neuroimaging methods. The network analysis of these databases have revealed principles of organization of the nervous system which are common across species.

For example, the corticocortical connectivity structure of the cat brain cortex is composed by 53 cortical areas and 826 axon fibers between them. The connections are weighted according to the axonal density of the projections [4,5]. The cat network was found to be organized into four clusters with func-

tional subdivisions: visual, auditory, somatosensory-motor, and frontolimbic. In the worm *C. elegans*, its neurons are arranged into modules, containing neural circuits which play a vital role in performing different functions: chemosensation, thermotaxis, mechanosensation, feeding, etc. [8,9]

The hierarchical structure revealed by the corticocortical connectivity of the cat suggests that a model for numerical simulations of this structure can be a clustered network, or a network formed by interacting subnetworks [10]. The subnetworks stand for the clusters and the neurons in subnetworks are connected with neurons belonging to the same cluster and other clusters as well [11,12]. Each such network has a connection architecture that is neither purely regular nor completely random, and we assume that they exhibit the so-called small-world (SW) property, since they display features of both regular and random lattices [13]. SW networks have been proposed to be an efficient solution for achieving modular and global information processing [14]. In fact, experimental studies in anesthetized cats have identified the SW properties in functional networks of cortical neurons using correlation analysis to identify functional connectivity [15].

SW neuronal networks are characterized by a small average geodesic distance between pairs of neurons and a large clustering coefficient. Regular lattices have large clustering values, but they fail to provide nonlocal interactions, which accounts for a large average distance between pairs of sites. In contrast, random networks have small average distance between neurons but fail to display high clustering [16]. This suggests that SW networks are in between these two limiting situations.

Networks with the SW property can be obtained from a regular lattice in which shortcuts are randomly inserted

\*Corresponding author: [viana@fisica.ufpr.br](mailto:viana@fisica.ufpr.br)

according to a given nonlocal shortcut probability [17]. In a clustered SW network both levels are described by this type of network, with different nonlocal shortcut probabilities. We thus have both intracluster and intercluster probabilities, related to the subnetwork describing one cluster and the connections among clusters, respectively. Such a hierarchical network can be used for the numerical investigation of many collective dynamical phenomena of neuroscientific interest [18,19]. There are also numerical studies of clustered scale-free networks, for which the connection probabilities follow a power-law scaling [20,21]. Scale-free networks exhibit highly connected neurons, or hubs, which are absent in our model.

The dynamical phenomenon in which we focus in this work is the synchronization of the bursting activity of neurons. There are evidences that partial synchronization may be related to a series of processes in the brain. Synchronized rhythms have been observed in EEG recordings of electrical brain activity and are regarded to be an important mechanism for neural information processing [22]. Experimental observations reveal synchronized oscillations in response to sensory stimuli in a variety of brain areas [23,24]. Such synchronized rhythms reflect the hierarchical organization of the brain and occur over a wide range of both spatial and temporal scales [25]. Certain neurons in the brain exhibit burst activity: bursts of multiple spikes followed by a rest state hyperpolarization. These bursting neurons are important in different aspects of brain function such as movement control and cognition [26–28].

If the neurons possess two distinct time scales, such as spiking and bursting, the bursts (slow time scale) tend to synchronize at smaller synaptic strengths [29,30]. We regard two or more neurons to be bursting in a synchronized manner if they start a given burst at nearly the same time, even though the fast spikes may not be synchronized. Bursting synchronization is related to neuron plasticity and memory via Hebbian plasticity and long-term potentiation [1]. Moreover, bursting synchronization has been found to be related with a number of abnormal brain rhythms, like Parkinson's disease and essential tremor [31]. In fact, suppression of bursting synchronization in specific regions of the brain has been proposed as a way to reduce abnormal neurological rhythms [32].

We want to analyze the collective dynamics of a clustered network of bursting neurons and give bounds for the smallest coupling strength needed to achieve global synchronization on the bursting scale. Many neuron models exhibit two time scales, ranging from differential equations such as the Hodgkin-Huxley [33], Hindmarsh-Rose [34], and Izhikevich [35] models to simpler two-dimensional maps such as the Rulkov model [36]. We have chosen the latter one, since its simplicity allows for extensive computer simulations of many neurons, but still retaining basic dynamical features of more complicated models.

In this paper we investigate bursting dynamics on SW clustered networks. Close to the global synchronized state the phase dynamics of the burst may be described, to a first order approximation, by a Kuramoto-like model [37]. Further investigations in the Kuramoto model allows us to determine the critical coupling strength for obtaining global bursting synchronization in terms of the probabilities of intracluster and intercluster connections. We show that the route to a global

synchronized state reveals two distinct types of transitions as a function of the intercluster probability. If the latter is small enough, then the transition to global synchronization is smooth, as opposed to higher values of the intercluster probability. In the latter case the network may present an abrupt transition to global synchronization.

This paper is structured as follows. In Sec. II we present the model for SW clustered networks, in which the individual neuron dynamics has a slow time scale representing bursting. Section III considers global phase synchronization of bursting neurons and also a discussion on partial phase synchronization. Section IV contains the phase reduction we perform to obtain a Kuramoto-like model of coupled phase oscillators. The transition to phase synchrony and its dependence on the cluster architecture is treated in Sec. V. The final section is devoted to our Conclusions.

## II. CLUSTERED SMALL-WORLD NETWORKS (NETWORKS OF NETWORKS)

### A. Connection architecture

Neuronal networks typically display the SW property [15,18]. We construct a clustered network with two hierarchical levels, a network composed by subnetworks. Each subnetwork is a SW network obtained from a regular one-dimensional lattice of neurons with periodic boundary conditions. Each neuron is connected to its nearest and next-to-nearest neighbors. Then we randomly add new connections among neurons in the lattice with a given intracluster probability  $p_i$  [17,38]. A small number of neurons in each subnetwork are additionally connected to neurons in other subnetworks. These intercluster connections are randomly chosen with an intercluster probability  $p_0$ . At this larger scale the network is not supposed to have the SW property, though, and it is more properly described as a random network (Erdős-Renyi).

We study a network composed of  $M$  SW subnetworks with  $L$  neurons each [Fig. 1(a)]. The two main properties characterizing each subnetwork are the average separation  $\ell$  between neurons, which is the average number of links necessary to connect two neurons, and the clustering coefficient  $C$ , defined as the average fraction of pairs of neighbors of a neuron that happen also to be neighbors of each other. In order to verify the SW property for each subnetwork, we have computed  $\ell$  and  $C$  as functions of the intracluster probability  $p_i$  [Fig. 1(b)].

In a SW network the average distance between neurons must be of the same order as for a random (Erdős-Renyi) graph,  $\ell \approx \ell_{\text{random}} \sim \ln N$ , whereas the clustering coefficient is much greater than for a random graph,  $C \gg C_{\text{random}} \sim 1/N$ . Hence, the results of Fig. 1(b) suggest that the SW property is well displayed when  $p_i \sim 10^{-2}$ . Our intra- and intercluster probabilities will be chosen using this procedure, depending on the network size used.

### B. Neuron bursting dynamics

Besides the spiking behavior of the action potential through the neuron membrane, a neuron has also a bursting activity, characterized by repeated spiking followed by quiescent periods [29]. Many neurons in the neocortex, hippocampus, thalamus, and cerebellum, among other examples, exhibit

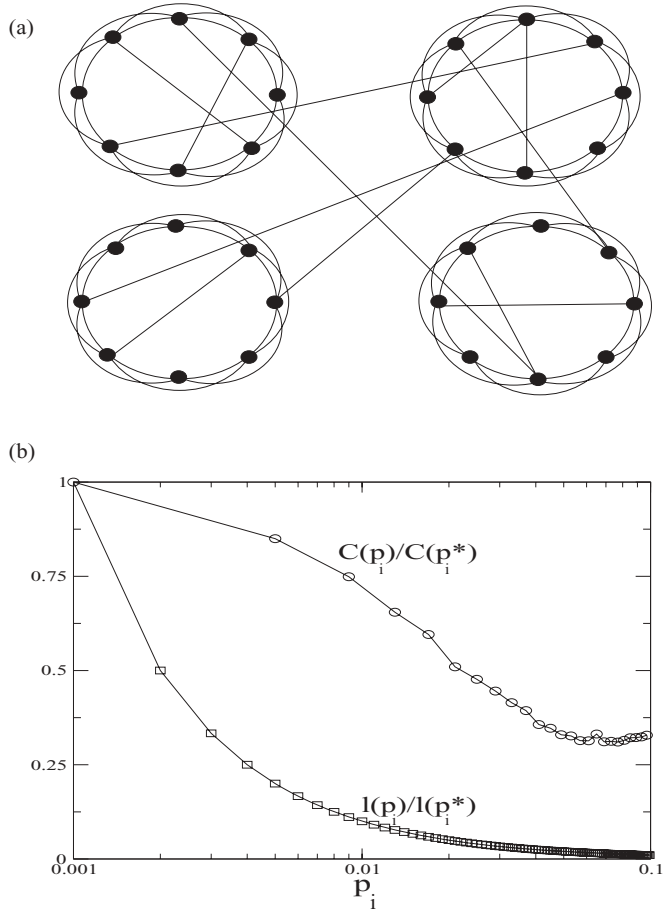


FIG. 1. (a) Schematic representation of a SW clustered network with  $M = 4$  clusters, each of them with  $L = 8$  nodes. (b) Normalized clustering coefficient (open circles) and normalized average separation between neurons (open squares) as a function of the intracluster probability  $p_i$  of nonlocal connections for a SW network with  $N = 100$  nodes and  $p^* = 10^{-3}$  is a reference probability.

autonomous or induced bursting [39]. Autonomous bursting is due to the interplay of fast ionic currents responsible for spiking activity and slower ionic currents that modulate the spiking activity [35]. It is currently thought that the bursting dynamics is essential to understand how a neuron performs computation and information processing [40].

The existence of both spiking and bursting activities introduces two distinct time scales in the neuron dynamics, requiring two different variables to model neuron dynamics: a fast (vector) variable  $\mathbf{x}$ , describing the action potential spikes, and a bursting (vector) variable  $\mathbf{y}$  representing the slow modulation of the spiking activity. Several mathematical models have been introduced to study this behavior, with either continuous (differential equations) or discrete time (maps) [34,41].

Since our work mainly aims to investigate the impact of connection properties of the network, we have chosen one of the simplest models which retain the essential features of spiking and bursting dynamics, the two-dimensional Rulkov map [42,43],

$$x(n+1) = f(x(n), y(n)) = \frac{\alpha}{1 + [x(n)]^2} + y(n), \quad (1)$$

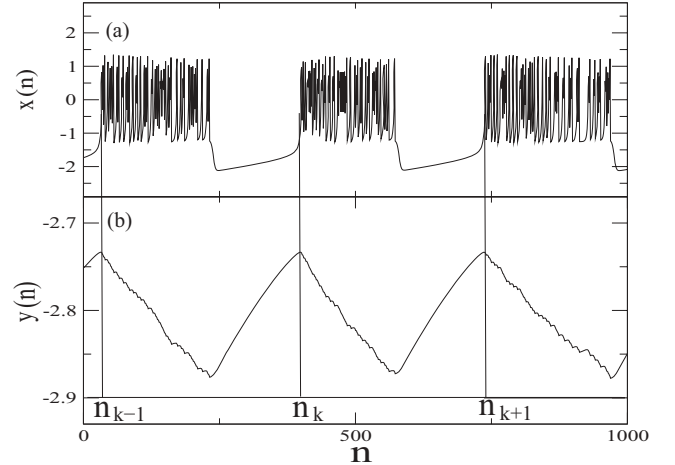


FIG. 2. Time evolution of the (a) fast  $x(n)$  and (b) slow  $y(n)$  variables in the Rulkov map (1) and (2) for  $\alpha = 4.1$ ,  $\sigma = \beta = 0.001$ .

$$y(n+1) = g(x(n), y(n)) = y(n) - \sigma x(n) - \beta, \quad (2)$$

where  $x(n)$  and  $y(n)$  are the fast and slow dynamical variables, respectively.

The parameter  $\alpha$  affects directly the spiking time scale and is chosen so that the time series of  $x(n)$  presents an irregular sequences of spikes [Fig. 2(a)]. Since neurons typically exhibit some diversity, we model this feature by choosing randomly some parameters over a limited range, as long as we still have a bursting regime. In our case we consider randomly the values of  $\alpha$  within the interval [4.1,4.4] according to a uniform distribution. The parameters  $\sigma$  and  $\beta$  take on small values, describing the slow time scale represented by bursts, in accordance with the results obtained to model the action of an external bias current and the synaptic inputs on an isolated neuron [42]. The slow variable  $y(n)$  is a slow modulation of the fast variable  $x(n)$  spiking behavior such that a given burst (i.e., the repeated sequence of spikes) begins when  $y(n)$  has a local maximum and terminates when it is at a local minimum [Fig. 2(b)]. The recovery of  $y(n)$  marks the quiescent period it takes before the next burst begins.

From Fig. 2(b) we see that the amplitude of the slow variable is less than 10% of that for the fast variable. Hence, in order to understand the existence of repeated bursting activity, we may approximate  $y(n)$  by a constant value  $\gamma$  in Eq. (1). The resulting one-dimensional map,  $x(n+1) = [\alpha/(1+x(n)^2)] + \gamma$ , can have one, two, or three fixed points  $x_{1,2,3}^*$ , depending on the value of  $\gamma$ . As the latter approaches a critical value  $\gamma_{SN}$ , the fixed points  $x_{1,2}^*$  (one stable and another unstable) undergo a saddle-node bifurcation; that is, for  $\gamma \gtrsim \gamma_{SN}$  the fixed points  $x_{1,2}^*$  disappear. For values of  $\gamma > \gamma_{CR}$  there is also a chaotic attractor that, provided  $\gamma_{CR} < \gamma < \gamma_{SN}$ , coexists with the stable fixed point attractor. Actually, at  $\gamma = \gamma_{CR}$  the chaotic attractor collides with the unstable fixed point  $x_1^*$  and is destroyed through a boundary crisis. The bursting regime appears to be due to a hysteresis behavior between the stable fixed point (quiescent evolution) and the chaotic oscillations (fast sequence of spikes) [41].

### C. Chemical synapses

Given the connection architecture we propose for the clustered network and the type of local neuron dynamics, the last ingredient in the model is the implementation of chemical synapses. Chemical synaptic connections represent most neuronal connections in the neocortex [44]. A depolarized presynaptic neuron releases chemical messengers (neurotransmitters) that bind to the receptors of the postsynaptic neurons. There are excitatory and inhibitory neurons that occur in an approximate 3 : 1 ratio in the cortex. For simplicity, we have chosen excitatory chemical synapses in our model. Inhibitory connections in the brain are known to be short-ranged and all the long-range connections are excitatory. Therefore, if inhibitory connections shall be included in a model like the present one, they should be only between neurons in the same subnetwork and connections between two subnetworks should be all excitatory.

The coupling can be implemented in the discrete-time model just described by forming a network, where  $x_i(n)$  and  $y_i(n)$  stand for the fast and slow variables, respectively, of the  $i$ th neuron ( $i = 1, 2, \dots, N$ ) at time  $n$ . In our clustered network we have  $N = ML$ , where  $M$  is the number of clusters and  $L$  is the number of neurons in each cluster (supposed to be equal for simplicity).

The coupling is performed on the fast variable  $x(i)$  in the form

$$x_i(n+1) = f(x_i(n), y_i(n)) + \varepsilon I_i(n), \quad (3)$$

$$y_i(n+1) = g(x_i(n), y_i(n)), \quad (4)$$

where the coupling term  $I_i(n)$  represents a total synaptic current to the  $i$ th neuron, which is the sum of spikes from all presynaptic neurons at time  $n$ , connected to  $i$  according to the connection topology chosen, and  $\varepsilon > 0$  is an overall coupling strength.

The response from the excitatory chemical synapses must include two effects: (i) a nonlinear response from the neuron and (ii) the difference between the membrane action potential of a postsynaptic neuron [which we represent by  $x(i)$ ] and a reversal potential  $V_s$ . Hence, we model the total synaptic current acting on a neuron as

$$I_i(n) = \sum_{j=1}^N a_{ij} S(x_j(n))(x_i(n) - V_s), \quad (5)$$

where  $a_{ij}$  is the connectivity matrix, whose elements are 1 or 0 if the postsynaptic neuron  $i$  and the presynaptic neuron  $j$  are (are not) connected. In our model of a clustered SW network the matrix is obtained from the procedure previously described in this section.

The reversal potential is chosen such that  $V_s > x_i(n)$  for any  $x_i(n)$ , in such a way that the chemical synapse is excitatory. The nonlinear response of the neuron is modeled by a static sigmoidal nonlinear input-output function with a threshold  $\lambda$  and a saturation parameter  $\Theta_s$  [45]

$$S(x) = \frac{1}{1 + e^{-\lambda(x - \Theta_s)}}, \quad (6)$$

where  $\Theta_s$  is chosen such a way that every spike within a single neuron burst can reach the threshold.

The model describing our neural network is thus

$$\begin{aligned} x_i(n+1) &= \frac{\alpha_i}{1 + [x_i(n)]^2} + y_i(n) \\ &+ \varepsilon \sum_{j=1}^{ML} a_{ij} \frac{x_i(n) - V_s}{1 + \exp[-\lambda(x_j(n) - \Theta_s)]}, \quad (7) \\ y_i(n+1) &= y_i(n) - \sigma x_i(n) - \beta. \quad (8) \end{aligned}$$

In the numerical simulations we shall use the following values for the parameters:  $\lambda = 10$ ,  $\Theta_s = -0.25$ ,  $V_s = 2.0$ ,  $\sigma = \beta = 0.001$ .

## III. PHASE OF BURSTING OSCILLATORS

### A. Bursting phase

Since we consider that the coupled neurons have small yet nonzero mismatches in their parameters, namely  $\alpha$ , they are nonidentical and, as a consequence, complete synchronization of chaotic spiking behavior is not possible. However, there may be a weaker form of synchronization, occurring when the coupled neurons burst approximately at the same times, with a similar matching of their quiescent periods as well. This type of behavior is referred to as *bursting synchronization*, which is actually a type of phase synchronization, as we explain in this section.

Bursting repeats itself with a slightly variable periodicity, which enables us to introduce a phase to describe the evolution during a given burst. Since neuron spiking and bursting have an underlying chaotic dynamics, a phase cannot always be unambiguously defined. Different ways to introduce a phase are possible, each one being chosen according to the particular case studied [46,47]. In our case, however, there is a simple way to define the phase  $\phi$  by considering that, at  $\phi = 0$ , a burst begins and evolves until, at  $\phi = 2\pi$ , another burst follows.

In practice, it suffices to track the time instants for which the slow variable  $y(n)$ , which presents nearly regular saw-teeth oscillations, has a local maximum, in well-defined instants of time we call  $n_k$  [Fig. 2(b)]. The duration of the chaotic burst,  $n_{k+1} - n_k$ , depends on the variable  $x(n)$  and, accordingly, fluctuates in an irregular fashion as long as  $x(n)$  undergoes a chaotic evolution [48]. We define a phase describing the time evolution within each burst, from  $n_k$  to  $n_{k+1}$ ,

$$\phi(n) = 2\pi k + 2\pi \frac{n - n_k}{n_{k+1} - n_k}, \quad (n_k \leq n < n_{k+1}), \quad (9)$$

where  $n_k$  denotes the time occurrence of the  $k$ th burst [49].

### B. Phase synchronization

In this way, when two or more neurons burst synchronously, their phases are approximately equal. The collective behavior of the network may also be captured by the network mean field,

$$\langle x \rangle_\mu(n) = \frac{1}{ML} \sum_{i=1}^{ML} x_i(n), \quad (10)$$

in such a way that the emergence of the collective behavior enhances the mean field dynamics. Specially, if the bursts are synchronized, the mean field exhibits large-amplitude



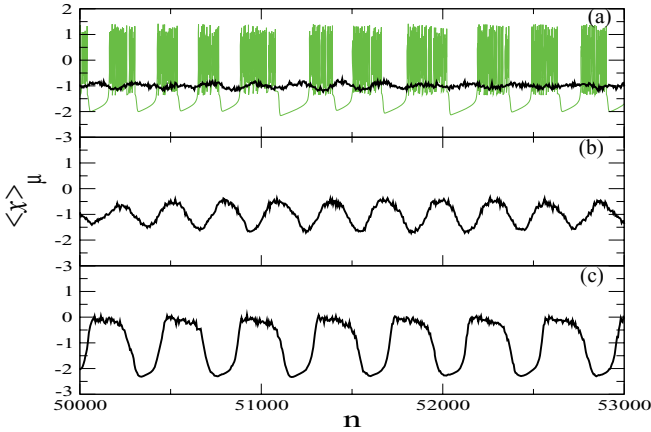


FIG. 3. (Color online) Behavior of the mean field for a clustered SW network as a function of the overall coupling parameter with fixed  $p_i = 10^{-2}$ ,  $p_o = 10^{-3}$ ,  $M = 4$ ,  $L = 100$ , and (a)  $\varepsilon = 0.01$ , (b)  $0.04$ , (c)  $0.10$ . The fast variable evolution of a selected neuron is the green (light gray) curve in (a).

oscillations, even though the spikes may be practically uncorrelated. On the other hand, if there is no synchronization, the contributions of individual neurons nearly cancel out and the mean field presents only small-amplitude noisy oscillations.

To illustrate the mean field dependence on the synchronization, we consider a clustered network with  $M = 4$  and  $L = 100$ , each subnetwork being a SW network with  $p_i = 10^{-2}$  and  $p_o = 10^{-3}$ . For small values of the overall coupling parameter  $\varepsilon$ , like  $0.01$ , the neurons burst in a nonsynchronized fashion. In fact, for this case the mean field is a noiselike signal, fluctuating around some value [Fig. 3(a)]. As the overall coupling increases, the mean field begins oscillating [Fig. 3(b)].

For higher values of coupling, the mean field oscillates in a similar way to the individual neurons [Fig. 3(c)]. Comparing these oscillations with those exhibited by uncoupled Rulkov neurons [such as depicted in Fig. 3(a)], we see that the mean field has a repeating behavior, first exhibiting fast fluctuations akin to the spikes produced by neurons, followed by a slower decay which is comparable with the quiescent period of bursting. Hence, the mean field bursting phase behaves similarly to the bursting phases of individual neurons. Complete equality is not possible, though, since the neurons have slight parameter mismatches. This state is called hereafter *global phase synchronization*. Near this state the mean field already echoes the bursting dynamics, while the fast oscillation due to the spike are filtered out. Intermediate states like in Fig. 3(b) exhibit partial phase synchronization. In fact, the difference between partial and complete synchronization is not so clear by inspecting Fig. 3, but we consider this point in more detail in the following.

### C. Order parameter

Global and partial phase synchronization can be distinguished from nonsynchronized states by a suitable numerical diagnostic, the complex order parameter introduced by Kuramoto [37]. Let  $\{\phi_i(n)\}_{i=1}^{ML}$  be the phases of the  $N$  neurons at time  $n$ . If we relate these phases to phasors, the order parameter

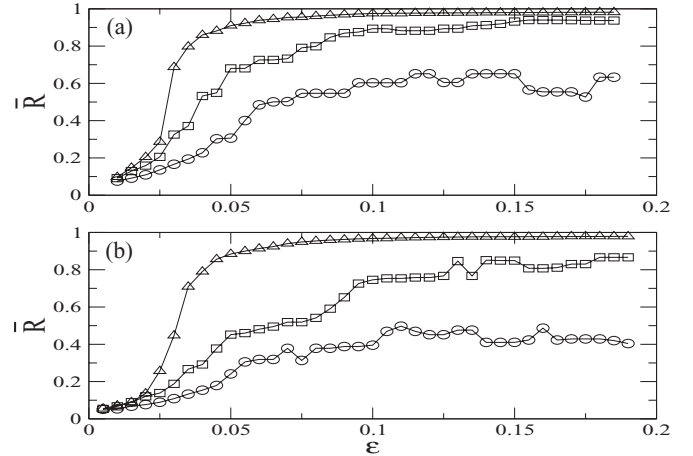


FIG. 4. Time averaged order parameter magnitude as a function of the overall coupling strength for  $p_i = 10^{-2}$ ,  $L = 100$ : (a)  $M = 2$  and (b)  $M = 4$ . In both figures we have  $p_o = 0$  (circles),  $p_o = 1.6 \times 10^{-4}$  (squares), and  $p_o = 2 \times 10^{-3}$  (triangles).

gives the magnitude  $R(n)$  and the angle  $\Psi(n)$  of a centroid phase vector:

$$z(n) = R(n)e^{i\Psi(n)} \equiv \frac{1}{N} \sum_{j=1}^N e^{i\phi_j(n)}, \quad (11)$$

and we usually compute its time-averaged magnitude  $\bar{R} = \lim_{T \rightarrow \infty} (1/T) \sum_{n=1}^T R(n)$ .

In a global phase synchronized state the bursting phases nearly coincide, and so their phasors add coherently and  $\bar{R}$  approaches unity. In contrast, if the state is completely nonsynchronized the bursting phases are practically uncorrelated, and the phasors cancel out, such that  $\bar{R} \approx 0$ . In the thermodynamical limit, that is, the limit of infinite neurons, we have  $\bar{R} = 0$ . Between values of  $\bar{R}$  thus characterize partial phase synchronized states.

We choose as the free parameters of our neural network model the overall coupling strength  $\varepsilon$  and the intra- and intercluster probabilities ( $p_i$  and  $p_o$ , respectively) related to the SW structure of the neural network. We compute  $\bar{R}$  for the network as a whole; that is, we set  $N = ML$  in Eq. (11).

In Fig. 4 we show the dependence of  $\bar{R}$  on  $\varepsilon$ , for fixed  $p_i = 10^{-2}$  and  $L = 100$  and varying  $p_o$ . In the case of  $M = 2$  clusters and a value of  $p_o$  large enough,  $\bar{R}$  [triangles in Fig. 4(a)] behaves in a similar way to a phase transition: For small  $p_o$  the neurons are very weakly coupled, and the bursting phases are practically nonsynchronized ( $\bar{R} \approx 1/M$ ). In particular, for the limiting case  $\varepsilon = 0$  results that  $\bar{R} \propto (ML)^{-1/2}$  so if  $L \gg 1$  or  $M \gg 1$ , then  $\bar{R} \approx 0$ .

When  $p_o = 0$ , the value of  $\bar{R}$  increases for nonzero  $\varepsilon$  and even reaches a value of approximately  $0.6$ . This is because, as  $\varepsilon$  increases, some clusters internally synchronize and, therefore, although they are not coupled, their dynamical behaviors look similar. Indeed, the mean field of each independent cluster would show oscillatory behavior. It is for these reasons that each cluster apparently get partially synchronized. This is not, though, a dynamical feature of the network, since the clusters are themselves uncoupled for  $p_o = 0$ .

As the  $\varepsilon$  increases,  $\bar{R}$  also increases in a sigmoid shaped curve, and  $\bar{R} \approx 1$  if  $\varepsilon$  is large. In practice, we get an almost global phase synchronized behavior if a threshold, say  $\bar{R} = 0.95$ , is achieved. The minimum  $\varepsilon$  to get to this threshold is called the critical coupling strength  $\varepsilon_c$ . If we decrease the intercluster probability  $p_o$ ,  $\bar{R}$  [squares in Fig. 4(a)] also increases with  $\varepsilon$ , but achieves global synchronization at a higher value than before.

It would appear that the effect of  $p_o$  could be only to postpone global phase synchronization, but we see that this is not the case, because for  $p_o = 0$  [circles in Fig. 4(a)] the network does not synchronize at all, even for larger  $\varepsilon$ . Increasing the number of clusters [Fig. 4(b)] leads essentially to the same conclusion. For a network that contains many clusters, a larger value of  $p_o$  is required to achieve global synchronization.

The existence of a critical coupling strength is a well-known feature of the Kuramoto model of globally coupled oscillators [50]. One of the advantages of this model is that it displays a transition to phase synchronization with a  $\varepsilon_c$  which can be predicted on quite general grounds. Hence, in order to study  $\varepsilon_c$  in clustered SW networks, we consider in Sec. IV a Kuramoto-type model of clustered networks in order to get an analytical prediction for  $\varepsilon_c$  in terms of  $p_i$ ,  $p_o$ , and  $N$ .

#### D. Dynamical modularity

Global phase synchronization of bursting neurons is a large-scale collective effect. On the other hand, in very large neuronal networks such global synchronization is not so interesting as transient synchronization between parts of the system. These situations are not captured by the mean field and are thus reflected as a weaker form of synchronization characterized by situations in which the subnetworks are locally synchronized but the network as a whole is still not. We may call this a modular, or partial, phase synchronization to distinguish it from the global synchronization we have discussed so far.

In this case we can restrict the computation of the mean field just to a few subnetworks (say, two of them). Hence, we may think of situations for which the modules (or subnetworks) are internally synchronized, but the global mean-field is still very weak. In such cases, synchronization of these modules may be far more interesting than synchronization of the entire network.

A quantitative characterization of clustered behavior in networks of networks is the dynamical modularity introduced by Gómez-Gardeñes *et al.* [51], which compares the degree of modular synchronization within subnetworks with the average dynamical correlation among the subnetworks. The average self-correlation of subnetworks is computed by using the order parameter magnitude for the subnetwork  $\mu$  only, denoted as  $R_{\mu\mu}$ , whereas the average intercluster cross-correlation is obtained from the order parameter magnitude computed by taking into account the subnetworks  $\mu$  and  $\nu$ , here denoted as  $\bar{R}_{\mu\nu}$ . In a network with  $M$  subnetworks the dynamical modularity  $D_M$  is defined as

$$D_M = \frac{\sum_{\mu} \bar{R}_{\mu\mu}/M}{\sum_{\mu \neq \nu} \bar{R}_{\mu\nu}/[M(M-1)]}. \quad (12)$$

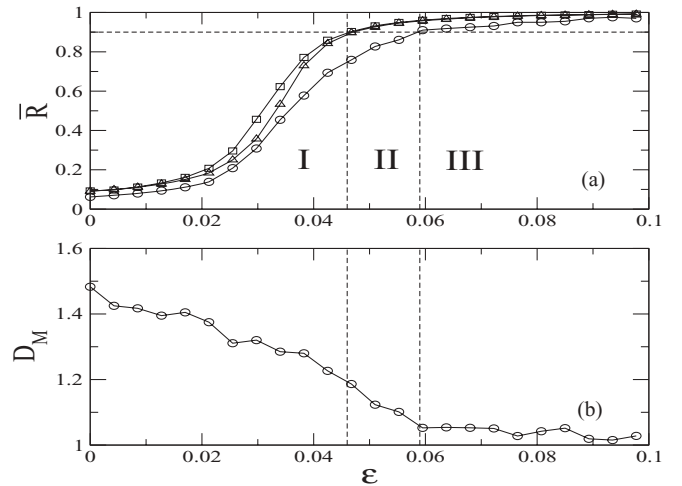


FIG. 5. (a) Time-averaged global order parameters and (b) dynamical modularity, as a function of the coupling strength, for a clustered network with  $M = 2$ ,  $L = 100$ ,  $p_i = 0.2$ , and  $p_o = 2.5 \times 10^{-3}$ . Results in (a) for each subnetwork are marked with triangles and squares, and for the entire network we used circles.

The dynamical modularity presents values above unity when the network presents a behavior consistent with clustered behavior and modular phase synchronization is possible. On the other hand,  $D_M$  is near (or less) to unity when the network behavior is not consistent with a clustered structure and global phase synchronization is more important.

In Figs. 5(a) and 5(b) we show  $\bar{R}$  and  $D_M$ , respectively, as a function of  $\varepsilon$ , for a clustered network of  $M = 2$  subnetworks. The squares and triangles in Fig. 5(a) stand for individual subnetworks, whereas the circles stand for the entire network. We can distinguish three  $\varepsilon$  intervals with qualitatively different behavior, in terms of the modular synchronization.

In Region I ( $0 < \varepsilon < 0.046$ ) all the values of  $\bar{R}$  are less than 0.95; hence, neither the networks nor the subnetworks are phase synchronized. The distinctive behavior of the clusters is captured by the dynamical modularity, since  $D_M \gtrsim 1.2$ . In Region II ( $0.046 \leq \varepsilon < 0.059$ ) the subnetworks have  $\bar{R} > 0.95$ ; thus, they are synchronized, but the entire network is not, although it is nearly synchronized; hence,  $D_M$  decreases and tends to values near unity. In fact, in Region III ( $0.059 \leq \varepsilon \leq 0.1$ ) all values of  $\bar{R}$  are higher than 0.95, indicating global phase synchronization and, accordingly,  $D_M$  takes on values near unity.

#### IV. REDUCTION TO A KURAMOTO-LIKE MODEL

Phase synchronization, unlike complete synchronization, has relatively fewer mathematical results on which we rely for rigorous statements. However, there is an outstanding exception represented by the Kuramoto model of globally coupled oscillators, for which the transition to synchronized behavior is fairly well understood in some cases [50]. It turns out that our system of coupled neurons can be subjected to a phase reduction such that it reduces to a Kuramoto-like model, and this allows us to use some results already developed for this class of models in clustered networks [52].

In Eq. (9) we defined a phase  $\phi(n)$  to describe the bursting activity. A similar phase, which we denote as  $\varphi(n)$ , can be also derived from the Kuramoto phase reduction techniques, which leads to an approximate phase equation to describe the collective phase dynamics of the neuron ensemble [37,53]. Moreover, we suppose that the time interval is short enough such that we may use a continuous time approximation, describing the phase change by a time derivative  $\dot{\phi}(t) \approx \phi(n+1) - \phi(n)$ .

### A. Phase reduction near global phase synchronization

Before considering the case of coupled bursting neurons, we present general results of phase reduction for a general  $D$ -dimensional flow, with some dynamical requirements which are mild enough to allow their application here. Let the dynamics of a single oscillator be given by a differential equation of the form

$$\frac{d\mathbf{x}}{dt} = \mathbf{F}(\mathbf{x}), \quad (13)$$

where  $\mathbf{x}$  is a  $D$ -dimensional vector. We assume that there is a stable period- $T$  orbit of this  $D$ -dimensional flow, such that

$$\mathbf{x}_0(t) = \mathbf{x}_0(t+T). \quad (14)$$

In this case, the ‘‘slow’’ dynamics along this periodic orbit can be described by a phase  $\varphi(\mathbf{x})$  such that

$$\frac{d}{dt}\varphi(\mathbf{x}) = \nabla_{\mathbf{x}}\varphi\mathbf{F}(\mathbf{x}) = 1. \quad (15)$$

Now let us consider a network of coupled oscillators with a slight mismatch in their parameters described by

$$\dot{\mathbf{x}}_i = \mathbf{F}(\mathbf{x}_i) + \mathbf{f}_i(\mathbf{x}_i) + \epsilon \sum_j a_{ij} \mathbf{V}(\mathbf{x}_i, \mathbf{x}_j), \quad (i = 1, 2, \dots, N), \quad (16)$$

where  $\mathbf{f}_i$  is different for each oscillator and stands for the vector field part containing slightly mismatched parameters,  $\epsilon$  is again the coupling strength,  $a_{ij}$  the adjacency (connectivity) matrix, and  $\mathbf{V}(\mathbf{x}_i, \mathbf{x}_j)$  is a coupling function.

From (15), the slow phase  $\varphi_i$  of the coupled oscillators is implicitly defined by the function

$$\mathbf{Z}(\varphi_i) = \nabla_{\mathbf{x}}\varphi(\mathbf{x}_0(\varphi_i)), \quad (17)$$

where  $\mathbf{x}_0$  is a period- $T$  stable orbit. The time evolution of the phase so defined is governed by

$$\dot{\varphi}_i = 1 + \epsilon \sum_j a_{ij} \mathbf{Z}(\varphi_i) \mathbf{V}(\mathbf{x}_i, \mathbf{x}_j) + \mathbf{Z}(\varphi_i) \mathbf{f}_i(\mathbf{x}_i), \quad (18)$$

for  $i = 1, 2, \dots, N$ .

By introducing the auxiliary phase  $\psi_i = \varphi_i - t$  and using a time average over a period  $T$ , keeping  $\psi_i$  fixed, we can write in a first-order approximation an equation governing the time evolution of  $\psi_i$ :

$$\dot{\psi}_i = \tilde{w}_i + \epsilon \sum_j a_{ij} \Gamma(\psi_i, \psi_j), \quad (19)$$

where

$$\tilde{w}_i = \frac{1}{T} \int_0^T \mathbf{Z}(t + \psi_i) \mathbf{f}_i(\mathbf{x}_i) dt, \quad (20)$$

$$\Gamma(\psi_i, \psi_j) = \frac{1}{T} \int_0^T \mathbf{Z}(t + \psi_i) \mathbf{V}(\mathbf{x}_0(t + \psi_i), \mathbf{x}_0(t + \psi_j)) dt, \quad (21)$$

play the roles of frequencies and coupling functions, respectively, for the auxiliary phases  $\psi_i$ .

If we are close to a global phase synchronized state, for which  $\varphi_i \approx \varphi_j$  for any pairs of oscillators  $(i, j)$ , we get an approximate form for the coupling function  $\Gamma$ . Introducing the time-dependent variable  $\zeta = t + \psi_j$  and supposing that  $\psi_j \ll T$  there results

$$\Gamma(\psi_i, \psi_j) = \frac{1}{T} \int_0^{T+\psi_j} \mathbf{Z}(\zeta + \psi_i - \psi_j) \times \mathbf{V}(\mathbf{x}_0(\zeta + \psi_i - \psi_j), \mathbf{x}_0(\zeta + \psi_j)) d\zeta. \quad (22)$$

By expanding the coupling function  $\mathbf{V}$  in a power series and assuming that  $\mathbf{Z}$  is nearly constant over the periodic orbit  $\mathbf{x}_0$ , we get

$$\Gamma(\psi_i, \psi_j) \approx a + b(\psi_i - \psi_j), \quad (23)$$

where

$$a = \frac{1}{T} \int_{\psi_j}^{\psi_j+T} \mathbf{Z} \mathbf{V}(\mathbf{x}_0(\zeta), \mathbf{x}_0(\zeta)) d\zeta, \quad (24)$$

$$b = \frac{1}{T} \int_{\psi_j}^{\psi_j+T} \mathbf{Z} (\nabla_{\mathbf{x}} \mathbf{V}(\mathbf{x}, \mathbf{y}))_{\mathbf{x}=\mathbf{y}=\mathbf{x}_0(\zeta)} \frac{\partial \mathbf{x}_0}{\partial \zeta} d\zeta, \quad (25)$$

Notice that this approximation holds whenever

$$\nabla_{\mathbf{x}} \mathbf{V}(\mathbf{x}, \mathbf{y}) \neq 0 \quad (26)$$

for any  $\mathbf{x}$  and  $\mathbf{y}$  belonging to the periodic orbit  $\mathbf{x}_0$ .

Substituting (23) into (19), we yield

$$\dot{\psi}_i \approx \tilde{w}_i + s_i a + \epsilon b \sum_j a_{ij} (\psi_i - \psi_j), \quad (27)$$

where  $s_i = \sum_j a_{ij}$  is the intensity of the  $i$ th node of the network. Since we are dealing with SW networks, which are almost regular—with the exception of some nonlocal shortcuts randomly added with a small probability—the intensities  $s_i$  present only a small variation over the network. Hence, we can take  $s_i$  as practically constant, that is, independent of  $i$ .

Moreover, since we are, by hypothesis, near a global phase synchronized state, the phase difference  $\psi_i - \psi_j$  is small enough to justify the replacement  $\psi_i - \psi_j \approx \sin(\psi_i - \psi_j)$ , in such a way that the equation governing the time evolution of the auxiliary phases (near a phase-synchronized situation) is a Kuramoto-like model,

$$\dot{\psi}_i \approx w_i + \epsilon \sum_j a_{ij} \sin(\psi_i - \psi_j), \quad (28)$$

where  $w_i = \tilde{w}_i + a s_i$  and  $\epsilon = \epsilon b$ .

### B. Phase reduction for bursting neurons

We next apply the general results for phase reduction near the phase-synchronized state to the case of bursting neurons,

provided some approximations are made. We can describe the dynamics of a single neuron by a differential equation like (13), where  $\mathbf{x}$  is a  $D$ -dimensional vector containing both the fast (spiking) and slow (bursting) dynamics. In addition,  $\mathbf{F}$  can be, for example, the Hindmarsh-Rose equations ( $D = 3$ ) or a similar model with two time scales.

For bursting neurons we have described a phase  $\phi$  by Eq. (9). Even though the spiking (fast) dynamics is chaotic and generally uncorrelated, numerical simulations show that there may be global phase synchronization even in this case. This phenomenon can be regarded as being a kind of phase coherence, which is a more general situation for it may hold even when a chaotic compact attractor  $\mathcal{A}$  exists in the phase space.

Let  $\Phi$  be the phase defined over  $\mathcal{A}$ , and let  $\tau$  be the return time of an orbit to the surface of section given by  $\Phi = 0$ . Taking for convenience  $\Phi(0) = 0$ , the phase is said to be coherent if

$$|\Phi(0) - \Phi(\tau)| < \eta \ll 1. \quad (29)$$

In this case, the orbit in  $\mathcal{A}$  is chaotic but it may resemble a periodic orbit for times less than  $t_{\max} \sim o(1/\eta)$ . If such a phase  $\Phi$  exists, then it is possible to introduce a coordinate change  $\Phi \rightarrow \phi$  such that  $\phi = 1 + \delta$ , where  $\delta$  is a noise term. We have chosen the model parameters so that the bursts are slightly irregular. Hence, the bursting phase defined in (9) is coherent in the mathematical sense given by (29).

The terms  $\mathbf{f}_i$  in Eq. (16), which are different for each neuron, stand for the vector field part containing the slightly mismatched parameters (which are, in the Rulkov map, the  $\alpha_i$ 's). Moreover, the sigmoid function (6) giving the nonlinear response of the chemical synapses is such that the condition (26) for applying the phase reduction procedure is satisfied. In particular, since the bursting dynamics is coherent near global phase synchronization, it is possible to introduce a coordinate change such that the phase of the  $i$ th neuron reads

$$\phi_i(t) = 1 + \psi_i(t) + \zeta_i(t), \quad (30)$$

where  $\psi_i$  satisfies a Kuramoto-like model (27) and  $\zeta$  is a noise term standing for small fluctuations caused on the bursting dynamics by the chaotic dynamics in the spiking behavior [46,54].

### C. Critical coupling for the global phase-synchronized state

Once we make a phase reduction such that the bursting phase satisfies Eq. (28), we can use recent theoretical results on clustered networks described by the Kuramoto model, obtained by Guan *et al.* [52]. We start from a modified version of the order parameter (11), which is called *local order parameter*, since it depends on the network site being considered

$$z_i = R_i e^{i\psi_i} \equiv \sum_{j=1}^N a_{ij} \langle e^{i\psi_j(n)} \rangle_n, \quad (i = 1, 2, \dots, N), \quad (31)$$

where  $a_{ij}$  is the adjacency matrix considered in the Kuramoto-like model (28), and  $\langle \dots \rangle$  stands for the time average (hence,  $z_i$  is already a time-averaged quantity).

Using this definition, Eq. (28) reads

$$\dot{\psi}_i \approx w_i - \varepsilon R_i \sin(\psi_i(n) - \Psi_i) + \varepsilon h_i(n), \quad (32)$$

where  $\Psi_i$  is the time-averaged phase of the  $i$ th node and

$$h_i(n) = \text{Im} \left[ e^{-i\psi_i(n)} \sum_{j=1}^N a_{ij} e^{-i\psi_j(n)} \langle e^{i\psi_j(n)} \rangle_n \right], \quad (33)$$

In the nearly phase-synchronized system, the latter quantity is the sum of  $s_i$  uncorrelated random terms ( $s_i$  is the intensity of the  $i$ th node) and can be neglected for SW networks where the sites are poorly connected in general.

The global phase-synchronized state is the stable fixed point of Eq. (32) without the term  $h_i(n)$ , which is

$$\psi_i^0 = \Psi_i + \arcsin \left( \frac{w_i}{\varepsilon R_i} \right). \quad (34)$$

For  $\varepsilon = \varepsilon_c$  we have  $\Psi_i \approx \Psi_j$  and the value of  $R$  for the  $i$ th node reads

$$R_i \approx \sum_{j=1}^N a_{ij} \sqrt{1 - \left( \frac{w_j}{\varepsilon_c R_j} \right)^2}. \quad (35)$$

This expression has been approximately evaluated in Ref. [52] in terms of the frequency distribution function  $g(w)$ . As we approach the global phase-synchronized state, this frequency distribution becomes increasingly narrow, and the square root in (35) reduces to  $R_j$  times a constant which does not depend on the intercluster probability  $p_0$ . In a clustered network the intracluster connections are dense and the intercluster connections are sparse, such that  $R_i \approx R_j$ .

Finally, the summation in (35) is evaluated in the following way: Since each node is connected to the nearest and next-to-nearest neighbors, a given node is connected with  $L - 5$  nodes in the same cluster with probability  $p_i$ . Moreover, this node is also connected with other  $N - L$  nodes from different clusters with probability  $p_o$ , for  $N = ML$ . Hence,

$$\sum_{j=1}^N a_{ij} = p_i(L - 5) + p_o(N - L),$$

and we get an analytical expression for  $\varepsilon_c$  with respect to the inter- and intracluster probabilities [52]

$$\varepsilon_c = \frac{C}{p_i(L - 5) + p_o(N - L)}, \quad (36)$$

where the constant  $C$  depends on the threshold value of the global order parameter. The latter is essentially the same as we defined in Eq. (11), since it holds for the entire network and not for a particular node. In our numerical computations we have used this threshold as a fitting parameter, namely  $\bar{R}_{\text{thresh}} = 0.95$ .

Fixing a given intercluster probability  $p_o$ , we compute the time-averaged order parameter as a function of  $\varepsilon$  and determine its critical value when  $\bar{R} \approx 0.95$ . In Fig. 6 we plot  $\varepsilon_c$  as a function of  $p_o$  for two different numbers of clusters, keeping both  $p_i$  and  $L$  constant. The solid lines represent the theoretical prediction given by Eq. (36), where  $C = 0.07$  for  $M = 2$  and  $C = 0.112$  for  $M = 4$  clusters.



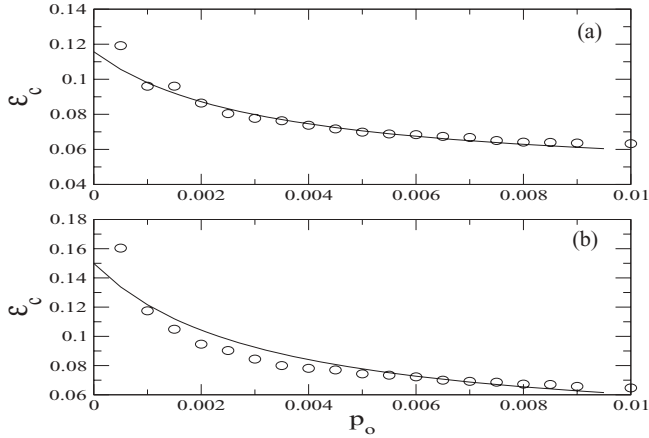


FIG. 6. Critical coupling strength for global phase synchronization of bursting neurons  $\varepsilon_c$  vs intercluster probability  $p_o$  for a network with  $L = 100$ ,  $p_i = 10^{-2}$ , and (a)  $M = 2$  and (b)  $M = 4$ . The circles are numerically determined from a threshold value of 0.95 for the global order parameter, whereas the solid lines stand for the theoretical prediction given by Eq. (36).

The theoretical prediction is in very good agreement with the numerical results for  $M = 2$  clusters and in good agreement for high intercluster probability in the case  $M = 4$ . In both cases  $\varepsilon_c$  decreases with  $p_o$ . In fact, the larger is  $p_o$ , the more connected are the bursting neurons in the network and thus the easier it is to get global phase synchronization. Hence,  $\varepsilon_c$  is expected to decrease with increasing  $p_o$ .

## V. INTERMITTENT TRANSITION TO PHASE SYNCHRONIZATION

The transition of our system to global phase synchronization occurs in an intermittent fashion: For  $\varepsilon$  just before its critical value  $\varepsilon_c$  the global order parameter, as a function of time, alternates between a state where it is near unity and another one for which it is substantially less than 1. Here it is also convenient to adopt a threshold value of 0.95 and consider as a *laminar state*, the interval for which  $R(n) > 0.95$ .

For  $\varepsilon$  smaller than  $\varepsilon_c$  these laminar states are relatively rare and  $R(n)$  takes on small values. However, as  $\varepsilon$  tends to  $\varepsilon_c$  these laminar states become more frequent until they subside for all times. In order to quantify this intermittent behavior, we introduce

$$F = \frac{1}{s} \sum_{n=1}^s \frac{N_n}{\Delta_n}, \quad (37)$$

where  $N_n$  is the number of time intervals for which  $R(n) > 0.95$  during a certain total time span  $\Delta_n$ . Since the SW networks were constructed probabilistically, we take an average over a number  $s$  of different configurations of the connections distributed with the determined probability  $p_o$ .

Thus,  $F$  can be interpreted as the fraction of global synchronization in a given time interval. If  $F = 1$  we have a permanent global phase-synchronized state, whereas any value less than unity represents an intermittent state. The value of  $F$  depends on the coupling strength  $\varepsilon$  and may present distinct behaviors according to the intercluster probability  $p_o$ . In Fig. 7 we depict the dependence of  $F$  on  $\varepsilon$  for two values of  $p_o$ .

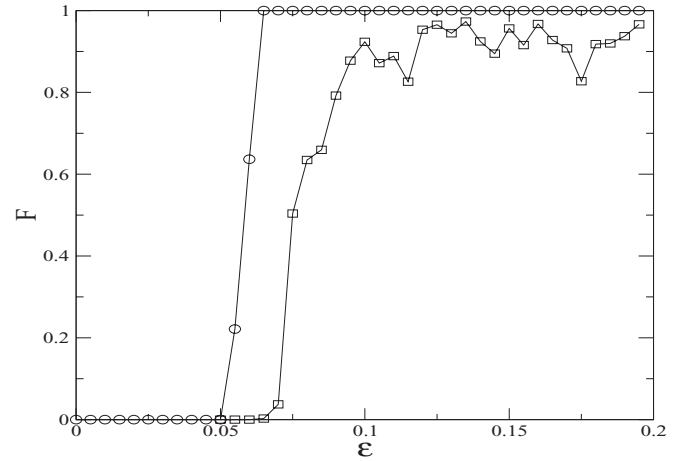


FIG. 7. Fraction of time where the clustered network has laminar states (order parameter higher than 0.95) vs the coupling strength for  $p_o = 10^{-1}$  (circles) and  $p_o = 10^{-2}$  (squares). The remaining parameters are  $L = 100$ ,  $M = 2$ ,  $p_i = 10^{-2}$ , and  $s = 20$ .

As a matter of fact, for small  $\varepsilon$  the value of  $F$  is so small that there are no laminar states at all; that is, no intermittency occurs. As we increase  $\varepsilon$  there is an abrupt transition to global phase synchronization beginning at  $\varepsilon_1 \approx 0.05$  and ending at  $\varepsilon_2 \approx 0.07$  (for  $p_o = 10^{-1}$ ). This kind of transition to global phase synchronization is similar in many aspects to the bubbling transition to synchronization, which occurs for coupled identical oscillators (where it is meant to describe complete synchronization, not just in the phases, though) [55].

The bubbling transition is based on the identification of the erratic behavior between laminar states as a chaotic transient, similarly to that occurring when a chaotic attractor suffers a crisis by collision with an unstable periodic orbit. This crisis generates an invariant nonattracting set, called *chaotic saddle* [56]. Trajectories in a chaotic saddle wander erratically but eventually decay to some other state. In the case of coupled chaotic oscillators, this state may be the synchronized state (or manifold, viewing this state in terms of the corresponding phase space).

A necessary condition for bubbling is that there is a chaotic attractor in the synchronized state [57]. The natural measure of this chaotic trajectory is supported by an infinite number of unstable periodic orbits embedded in this chaotic trajectory. If all of these periodic orbits are transversely stable, that is, they are stable with respect to infinitesimal displacements along transversal directions, there are no episodes of non-synchronized behavior and the system stays for an arbitrary time in the synchronized state. This explains the absence of nonsynchronized behavior for  $\varepsilon > \varepsilon_2$  in Fig. 7.

However, in spite of some unstable orbits embedded in the synchronized state being transversely unstable, the synchronized state itself may remain transversely stable. Therefore, trajectories off but very near the synchronized state experience intermittent excursions due to the presence of the chaotic saddle, but eventually decay to the synchronized state. This explains the existence of intermittent behavior for  $\varepsilon_1 < \varepsilon < \varepsilon_2$  in Fig. 7.

As the synchronized state as a whole loses transversal stability, though, the trajectories stay for an arbitrarily long

time in the chaotic saddle experiencing an erratic behavior, and no laminar states exist whatsoever. This corresponds to the absence of laminar states when  $\varepsilon < \varepsilon_1$  (Fig. 7). We point out, however, that this explanation is essentially qualitative, since bursting neurons with slightly mismatched parameters are not expected to display complete synchronization, but rather phase synchronization (which is a milder form of synchronization). In this case, this description is not so simple, since we cannot rigorously define a synchronization manifold with the stability properties necessary to apply the bubbling transition scenario.

The limitations inherent to this description are apparent in Fig. 7, when we consider a smaller intercluster probability, namely  $p_o = 10^{-2}$ . For such a network the intercluster connections are more sparse than in the previous case, and we did not observe global phase synchronization (at least for a 0.95 threshold for the global order parameter). In spite of this, we can still observe traces of a bubbling transition, since there is a  $\varepsilon_1 \approx 0.07$ . Moreover, if we lower the order parameter threshold, we could still give meaning to a  $\varepsilon_2$ , but this time with no obvious connection with the previous case.

Instead of invoking a bubbling transition scenario, however, we can also regard the behavior of  $F$  for small  $p_o$  as a qualitatively distinct kind of transition. Whereas in the larger  $p_o$  case the transition was abrupt (thanks to the bubbling mechanism), in the small  $p_o$  case the transition is smooth. The latter behavior can be understood heuristically in terms of the synchronization properties of each isolated cluster.

If  $p_o$  is small enough, each cluster is almost independent. Hence, each subnetwork tends to synchronize by itself. So, as we increase  $\varepsilon$ , each cluster becomes intermittently synchronized and only after such a condition is achieved we may observe global synchronization, what leads to a smooth transition. On the other hand, if  $p_o$  is large, then the collective dynamics of each subnetwork is strongly affected by the rest of the network. Hence, when phase synchronization occurs in one subnetwork, this effect quickly spreads over the whole network, leading to an abrupt transition. In this situation the bubbling scenario may hold, since it was originally conceived for a single network.

## VI. CONCLUSIONS

We have presented a clustered network model for bursting neurons. The clustered structure is a prototype for a modular structure of the cortex, as laboratory evidence suggests for mammals like cats or macaque monkeys. Given the fact that chemical synapses are dominant for neuronal networks, we have described this clustered network as having the SW property, and for the individual neuron dynamics, we have chosen a two-dimensional map presenting evolution over both fast (spiking) and slow (bursting) time scales.

We have described a kind of collective behavior of the clustered network called global phase synchronization. Since we have chosen slightly different neurons there cannot be complete synchronization of chaotic spiking. However, since neurons spike repeatedly over a burst, they may synchronize the times they start to burst collectively. The bursting can be given a phase, such that the collective effect is phase synchronization.

A clustered SW network has two kinds of connection probabilities: inter- and intracluster. We have presented numerical results that support the conclusion that global phase synchronization is possible only if the intercluster probability is large enough. Then the transition from nonsynchronized to synchronized behavior is abrupt, and it occurs for a coupling strength larger than a critical value.

This critical value can be theoretically predicted by considering a clustered network where the coupled phase oscillators obey a Kuramoto-like model. We have performed such a phase reduction for the bursting neurons and have yielded a Kuramoto-like model with the required properties. In this case the numerical results we have yielded for the critical coupling strength are in good agreement with the theoretical prediction given by the Kuramoto-like model.

We have also shown that, as we approach the transition to global phase synchronization, the system undergoes intermittent excursions between the synchronized and nonsynchronized states. We have conjectured, based on results valid for complete synchronization of chaos, that this is due to a bubbling transition whose underlying dynamics is the presence of a synchronized state and a chaotic nonattracting invariant set in the phase space.

In the bubbling transition the synchronized state is thought of as a chaotic attractor containing infinitely many unstable periodic orbits. If some of these orbits become transversely unstable, intermittency between bursts and laminar states occurs due to the existence of the chaotic saddle. A permanent synchronized state would be possible only if no periodic orbit is transversely unstable.

On the other hand, if the intercluster probability is too small, this scenario of an abrupt transition to global synchronization may not apply, and we have a smooth transition to synchronization. In this scenario, the clusters are so weakly connected that global synchronization for the network is achieved only after all the clusters (subnetworks) have reached a phase-synchronized behavior. In this smooth transition case the bubbling scenario does not apply in its original form.

Our results suggest that phase synchronization is a phenomenon that can occur in models of neuronal networks, with distinctive characteristics with respect to the more usually considered complete synchronization. The latter, although being mathematically easier to describe and with many rigorous results, are somewhat idealized behaviors that are not likely to occur in realistic neuronal network. Phase synchronization, on the other hand, being a milder form of synchronized behavior, is more likely to occur in neuronal networks and has a robust characterization, although rigorous mathematical results are scarce. One of them though, is the transition to synchronized behavior in the Kuramoto model, which turns out to be a reduced model of more complex neuronal networks, as we have shown in our paper.

One important improvement to the present model would be the inclusion of inhibitory connections, since it is estimated that 25% of the synapses in the connectome are inhibitory. It is believed that the interplay of excitatory and inhibitory neurons is what generates the typical oscillations observed in the EEG data (e.g.,  $\alpha$  and  $\beta$  rhythms). That is the basis of the neural-mass models. With inhibitory neurons we might observe oscillations within each of the subnetworks, including

yet another time scale. However, this will probably depend in the particular position and connections between the neurons within each of the SW subnetworks.

#### ACKNOWLEDGMENTS

This work was made possible through partial financial support from the following Brazilian research agen-

cies: CNPq, CAPES, and Fundação Araucária. G. Zamora-López and J. Kurths are supported by the Federal Ministry of Education and Research, Germany (BCCN2, Grant No. 01GQ1001A), and the Deutsche Forschungsgemeinschaft, research group FOR 868 (Contract No. KU837/23-2). T.P. is supported by Leverhulme Trust Grant No. RPG-279.

- 
- [1] G. Buzsáki, *Rhythms of the Brain* (Oxford University Press, London, 2006).
- [2] C. C. Hilgetag and M. Kaiser, in *Lectures in Supercomputational Neuroscience (Dynamics in Complex Brain Networks)*, edited by P. B. Graben, C. Zhou, M. Thiel, and J. Kurths (Springer, Berlin-Heidelberg-New York, 2008).
- [3] G. Zamora-López, C. Zhou, and J. Kurths, *Front. Neurosci.* **5**, 83 (2011).
- [4] J. W. Scannell and M. P. Young, *Curr. Biol.* **3**, 191 (1993).
- [5] J. W. Scannell, C. Blakemore, and M. P. Young, *J. Neurosci.* **15**, 1463 (1995).
- [6] C. C. Hilgetag, G. A. Burns, M. O'Neill, J. W. Scannell, and M. P. Young, *Philos. Trans. R. Soc. London B* **355**, 91 (2000).
- [7] C. C. Hilgetag and M. Kaiser, *Neuroinformatics* **2**, 353 (2004).
- [8] A. Arenas, A. Fernández, and S. Gómez, *Lect. Notes Comput. Sci.* **515**, 9 (2008).
- [9] R. K. Pan, N. Chatterjee, and S. Sinha, *PLoS ONE* **5**, e9240 (2010).
- [10] G. Zamora-López, C. Zhou, and J. Kurths, *Chaos* **19**, 015117 (2009); *Front. Neuroinf.* **4**, 1 (2010).
- [11] M. Zhao, C. Zhou, J. Liu, and C. H. Lai, *Phys. Rev. E* **84**, 016109 (2011).
- [12] S.-J. Wang, C.-C. Hilgetag, and C. S. Zhou, *Front. Comput. Neurosci.* **5**, 30 (2011).
- [13] D. J. Watts, *Small Worlds* (Princeton University Press, Princeton, 2000).
- [14] M. Kaiser, M. Görner, and C.-C. Hilgetag, *New J. Phys.* **9**, 110 (2007).
- [15] S. Yu, D. Huang, W. Singer, and D. Nikolic, *Cereb. Cortex* **18**, 2891 (2008).
- [16] D. J. Watts and S. H. Strogatz, *Nature (London)* **393**, 409 (1998).
- [17] M. E. J. Newman and D. J. Watts, *Phys. Lett. A* **263**, 341 (1999).
- [18] P. Hagmann, M. Kuran, X. Gigandet, P. Thiran, V. J. Wedeen, R. Mueli, and K. Thiran, *PLoS ONE* **2**, e597 (2007).
- [19] X. Sun, J. Lei, M. Perc, J. Kurths, and G. Chen, *Chaos* **21**, 016110 (2011).
- [20] D. R. Chialvo, *Physica A* **340**, 756 (2004); O. Sporns, D. R. Chialvo, M. Kaiser, and C. C. Hilgetag, *Trends Cognit. Sci.* **8**, 418 (2004); V. M. Eguiluz, D. R. Chialvo, G. A. Cecchi, M. Baliki, and A. V. Apkarian, *Phys. Rev. Lett.* **94**, 018102 (2005).
- [21] Y. Hao, Y. Gong, L. Wang, X. Ma, and C. Yang, *Chaos Solitons Fractals* **44**, 260 (2011).
- [22] E. Salinas and T. J. Sejnowski, *Nat. Neurosci.* **2**, 539 (2001).
- [23] E. Rodriguez, N. George, J. P. Lachaux, J. M. B. Renault, and F. J. Varela, *Nature (London)* **397**, 430 (1999).
- [24] P. Fries, J. H. Reynolds, A. E. Rorie, and R. Desimone, *Science* **29**, 1560 (2001).
- [25] C. J. Stam and E. A. Bruin, *Hum. Brain Mapp.* **22**, 97 (2004).
- [26] W. Schultz, *J. Neurophysiol.* **80**, 1 (1998).
- [27] A. S. Freeman, L. T. Meltzer, and B. S. Bunney, *Life Sci.* **36**, 1983 (1985).
- [28] A. A. Grace and B. S. Bunney, *Neuroscience* **4**, 2877 (1984).
- [29] M. Dhamala, V. K. Jirsa, and M. Ding, *Phys. Rev. Lett.* **92**, 028101 (2004).
- [30] T. Pereira, M. S. Baptista, and J. Kurths, *Eur. Phys. J. Spec. Top.* **146**, 155 (2007).
- [31] M. Rosenblum and A. Pikowsky, *Phys. Rev. E* **70**, 041904 (2004).
- [32] C. A. S. Batista, S. R. Lopes, R. L. Viana, and A. M. Batista, *Neural Networks* **23**, 114 (2010).
- [33] A. L. Hodgkin and A. F. Huxley, *J. Physiol.* **117**, 500 (1952).
- [34] J. L. Hindmarsh and R. M. Rose, *Proc. R. Soc. London* **221**, 87 (1984).
- [35] E. M. Izhikevich, *Dynamical Systems in Neuroscience: The Geometry of Excitability and Bursting* (The MIT Press, Cambridge, 2007).
- [36] N. F. Rulkov, *Phys. Rev. Lett.* **86**, 183 (2001); *Phys. Rev. E* **65**, 041922 (2002).
- [37] Y. Kuramoto, *Chemical Oscillations, Waves and Turbulence* (Dover, New York, 2003).
- [38] A. M. Batista, S. E. de S. Pinto, R. L. Viana, and S. R. Lopes, *Physica A* **322**, 118 (2003).
- [39] E. M. Izhikevich, *Int. J. Bifurcat. Chaos* **10**, 1171 (2000).
- [40] E. M. Izhikevich, N. S. Desai, E. C. Walcott, and F. C. Hoppensteadt, *Trends Neurosci.* **26**, 161 (2003).
- [41] B. Ibarz, J. M. Casado, and M. A. F. Sanjuán, *Phys. Rep.* **501**, 1 (2011).
- [42] N. F. Rulkov, I. Timofeev, and M. Bazhenov, *J. Comput. Neurosci.* **17**, 203 (2004).
- [43] G. Schmidt, G. Zamora-López, and J. Kurths, *Int. J. Bifurcat. Chaos* **20**, 859 (2010).
- [44] L. Zemanová, C. Zhou, and J. Kurths, in *Lectures in Supercomputational Neuroscience (Dynamics in Complex Brain Networks)*, edited by P. B. Graben, C. Zhou, M. Thiel, and J. Kurths (Springer, Berlin-Heidelberg-New York, 2008).
- [45] H. Sompolinsky, A. Crisanti, and H. J. Sommers, *Phys. Rev. Lett.* **61**, 259 (1988).
- [46] K. Josić and D. J. Mar, *Phys. Rev. E* **64**, 056234 (2001).
- [47] T. Pereira, M. S. Baptista, and J. Kurths, *Phys. Lett. A* **362**, 159 (2007).
- [48] C. A. S. Batista, A. M. Batista, J. A. C. de Pontes, R. L. Viana, and S. R. Lopes, *Phys. Rev. E* **76**, 016218 (2007).
- [49] M. V. Ivanchenko, G. V. Osipov, V. D. Shalfeev, and J. Kurths, *Phys. Rev. Lett.* **93**, 134101 (2004).

- [50] J. A. Acebrón, L. L. Bonilla, C. J. P. Vicente, F. Ritort, and R. Spigler, *Rev. Mod. Phys.* **77**, 137 (2005).
- [51] J. Gómez-Gardeñes, G. Zamora-López, Y. Moreno, and A. Arenas, *PLoS ONE* **5**, e12313 (2010).
- [52] S. Guan, X. Wang, Y.-C. Lai, and C.-H. Lai, *Phys. Rev. E* **77**, 046211 (2008).
- [53] C. Liu, R. Weaver, S. H. Strogatz, and S. M. Reppert, *Cell* **91**, 855 (1997).
- [54] A. S. Pikowsky, M. G. Rosenblum, G. Osipov, and J. Kurths, *Physica D* **104**, 219 (1997).
- [55] P. Ashwin, J. Buescu, and I. Stewart, *Phys. Lett. A* **193**, 126 (1994); S. C. Venkataramani, B. R. Hunt, and E. Ott, *Phys. Rev. E* **54**, 1346 (1996).
- [56] E. Rosa, E. Ott, and M. H. Hess, *Phys. Rev. Lett.* **80**, 1642 (1998).
- [57] R. L. Viana, C. Grebogi, S. E. de S. Pinto, S. R. Lopes, A. M. Batista, and J. Kurths, *Physica D* **206**, 94 (2005).